Optics Letters

Giant two- to five-photon absorption in $CsPbBr_{2.7}I_{0.3}$ two-dimensional nanoplatelets

Junzi Li,[1] Fuli Zhao,[2,3] Shuyu Xiao,[1] Jiaji Cheng,[1,4] Xin Qiu,[1] Xiaodong Lin,[1] Rui Chen,[3,5] and Tingchao He[1,6]

[1]College of Physics and Optoelectronic Engineering, Shenzhen University, Shenzhen 518060, China
[2]College of Arts and Science, Shanghai Dianji University, Shanghai 201306, China
[3]Department of Electrical and Electronic Engineering, Southern University of Science and Technology, Shenzhen 518055, China
[4]School of Materials Science and Engineering, Hubei University, Wuhan 430062, China
[5]e-mail: chenr@sustech.edu.cn
[6]e-mail: tche@szu.edu.cn

Received 28 May 2019; revised 7 July 2019; accepted 7 July 2019; posted 9 July 2019 (Doc. ID 368755); published 31 July 2019

$CsPbBr_{2.7}I_{0.3}$ two-dimensional (2D) nanoplatelets (NPs) with emission wavelengths of 469 nm and 527 nm were synthesized and characterized. Femtosecond transient absorption spectra revealed hot carrier cooling times of ~368 fs and ~438 fs for 469 nm and 527 nm 2D NPs, respectively. Importantly, the 2D NPs exhibit giant two-, three-, four-, and five-photon absorption cross-sections, reaching $\sim 4.1 \times 10^{6}$ GM at 830 nm, $\sim 2.3 \times 10^{-74}$ cm^6 s^2 photon^{-2} at 1300 nm, 2.06×10^{-104} cm^8 s^3 photon^{-3} at 1600 nm, and 1.50×10^{-136} cm^{10} s^4 photon^{-4} at 2200 nm, respectively, which are 3–8 orders of magnitude larger, compared to specially designed organic molecules.

https://doi.org/10.1364/OL.44.003873

In the past decade, with the development of nonlinear optics and multiphoton fluorescence imaging, multiphoton absorption (MPA) enabled many technically important applications such as *in vivo* imaging, photodynamic therapy, and nonlinear optoelectronics [1,2]. An imaging system based on the MPA principle can obtain deeper penetration depth in living organisms and reduce background signal, while MPA in the near infrared region (NIR) is important for various nonlinear optoelectronic devices. Two- and three-photon absorption (2PA and 3PA) properties of various materials have been widely investigated [1]. Many kinds of organic molecules and semiconductor nanocrystals (NCs) with strong 2PA and 3PA were designed and synthesized. Compared to other semiconductor NCs, the characterization of MPA in perovskite NCs remains unsatisfactory. Sun *et al.* reported MPA of $CsPbBr_3$ NCs and their multiphoton-excited-stimulated emission for the first time [3]. Subsequently, some groups investigated MPA of various perovskite NCs [4–8]. Worth nothing is that four- and five-photon absorption (4PA and 5PA) of perovskite NCs has not been well addressed. Only 4PA and 5PA of multidimensional core-shell halide perovskites was reported by Sum *et al.* [4]. However, the synthesis process of such core-shell NCs is somewhat complicated. Hence, it is of very high interest to synthesize novel perovskite NCs with strong 4PA and 5PA, which also must have the advantages of high stability and easy synthesis.

Among various perovskite NCs, two-dimensional perovskite NPs (2D NPs) exhibit much stronger quantum confinement effects than their cubic counterparts; thus, they yielded a new category of photonic materials for various applications [9]. Of the various perovskite 2D NPs available, all-inorganic NPs with applications in nonlinear optics and optoelectronic devices, i.e., $CsPbX_3$ (X = Br, Cl, I), have attracted strong interest, because they exhibit significantly higher chemical stability than their widely studied organic/inorganic hybrid counterparts [10]. In particular, perovskite 2D NPs are advantageous in that their thicknesses can be controlled with atomic precision. They also exhibit high exciton-binding energies, which aid in light-emitting applications and other fields currently being explored [9]. In addition, perovskite 2D NPs are expected to exhibit special optoelectronic properties based on their MPA characteristics. However, there is no sufficient research on the MPA characteristics of all-inorganic perovskite 2D NPs, especially for four- and five-photon absorption (4PA and 5PA).

The main objective of this work was to confirm strong MPA in perovskite 2D NPs, especially 4PA and 5PA in NIR (1600–1800 nm and 2200–2400 nm, pulse width: 100 fs), owing to their strong 2D quantum confinement effect. This may be important for comprehensive understanding of their intrinsic photophysical properties and for broadening the potential for various applications. Since the 2PA and 3PA of $CsPbBr_3$ 2D NPs were reported in Ref. [8] and $CsPbI_3$ 2D NPs being very unstable, we selected $CsPbBr_{2.7}I_{0.3}$ 2D NPs as the studied target in this work.

Two types of $CsPbBr_{2.7}I_{0.3}$ 2D NPs were synthesized using the procedures reported in Ref. [11], and their morphologies were analyzed via transmission electron microscopy (TEM) [Figs. 1(a) and 1(b)]. The 2D NPs had thicknesses of ~2.4 nm and ~3.6 nm, which correspond to four- and six-unit cells, respectively. The lateral dimensions of the 2.4-nm-thick 2D NPs were ~8.7 nm and ~17.2 nm in the x and y directions, respectively. For the 3.6-nm-thick 2D NPs, the relevant values were

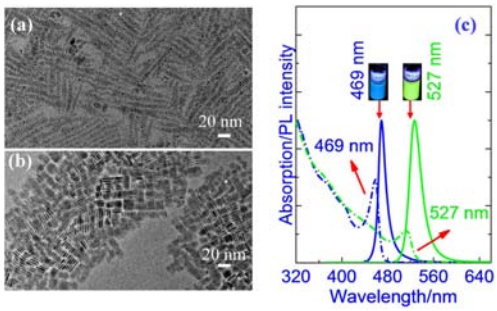

Fig. 1. TEM images of the (a) 469 nm and (b) 527 nm 2D NPs. (c) UV-Vis/PL spectra of the 469 nm and 527 nm 2D NPs. Insets: fluorescence photographs of the 469 nm and 527 nm 2D NPs, taken for the 365 nm UV irradiation.

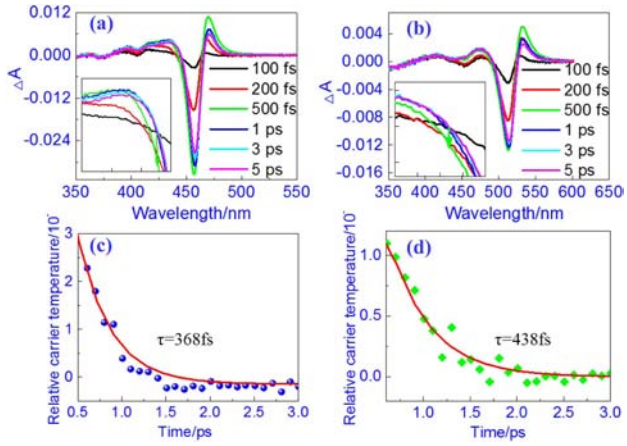

Fig. 2. fs-TA spectra of the (a) 469 nm and 527 nm, (b) 2D NPs, for the 350 nm excitation. The inset indicates hot carrier cooling above the band gap. Carrier cooling dynamics extracted from spectral evolution in the early picosecond time scale for the (c) 469 nm and (d) 527 nm 2D NPs.

~14.8 nm and ~23.5 nm, respectively. Their respective first exciton absorption peaks occurred at ~457 nm and ~513 nm, while their corresponding photoluminescence (PL) spectra peaks were at ~469 nm and ~527 nm, respectively. Hence, the 2.4-nm-thick 2D NPs were referred to as 469 nm 2D NPs, while the 3.6-nm-thick 2D NPs were abbreviated as 527 nm 2D NPs. In addition, both the 469 nm and 527 nm 2D NPs exhibited sharp exciton absorption and narrow emission bands, as well as small Stokes shifts, indicating significant 2D quantum confinement effects. The absolute PL quantum yields of the 469 nm and 527 nm 2D NPs were determined to be 3.1% and 7.6%, respectively. Perovskite 2D NPs have large surface-to-volume ratios, which make them susceptible to surface defects, resulting in PL quantum yields that are typically quite low [12].

The femtosecond-transient absorption (fs-TA) spectra of the 469 nm and 527 nm 2D NPs were measured to investigate their carrier cooling processes [13,14]. Fundamental studies of the 2D NP hot carrier relaxation dynamics are important for applications such as optoelectronic devices and solar cells [15]. In the fs-TA spectra, photoinduced absorption features form a multimodal structure, indicating that the 2D NPs exhibit a strong 2D quantum confinement effect [Figs. 2(a) and 2(b)]. For the 469 nm and 527nm 2D NPs, the hot carrier cooling times were 368 fs and 438 fs, respectively, with the carrier densities of 1.51×10^{18} cm^{-3} and 3.64×10^{17} cm^{-3}, respectively [Figs. 2(c) and 2(d)]. The carrier cooling times of the 2D NPs were comparable to the relevant values for many materials used for solar cells [16], including $CH_3NH_3PbI_3$ films [17] and CdS microplates [18]. The slow hot carrier cooling in 2D NPs indicates their small energy loss in optoelectronic device applications [16].

The linear absorption cross-section (σ_{lin}) of perovskite NCs is very important for determining their molar concentrations. However, owing to significant difference between the values of σ_{lin} determined using different methods, the deviation of the measured values of the 2PA cross-section in the same perovskite NCs can reach 1 order of magnitude [1,4,5]. Here, we used the fs-TA spectrum to obtain single-photon ground-state bleaching (GSB) signals for different excitation intensities, which can be used for estimating the linear absorption cross-sections of the 469 nm and 527 nm 2D NPs.

Figures 3(a) and 3(b) illustrate the relaxation curves of the GSB signals of the 469 nm and 527 nm 2D NPs, for different excitation intensities. After a rapid Auger effect, the decay processes in the 2D NPs contained only a single exciton process in the following period, which was further confirmed by noting that the dynamic curves for different excitation light intensities are parallel to each other when the time delay is >0.5 ns. The variation of the GSB signal amplitude for different excitation intensities can be described by the following equation:

$$-A(I/I_0) = -A_{max}[1 - e^{-(I/I_0)\cdot\sigma_{lin}\cdot I_0}], \quad (1)$$

where $A(I/I_0)$ represents the GSB signal amplitude of the 2D NPs after a long time delay, and I_0 is the minimal excitation

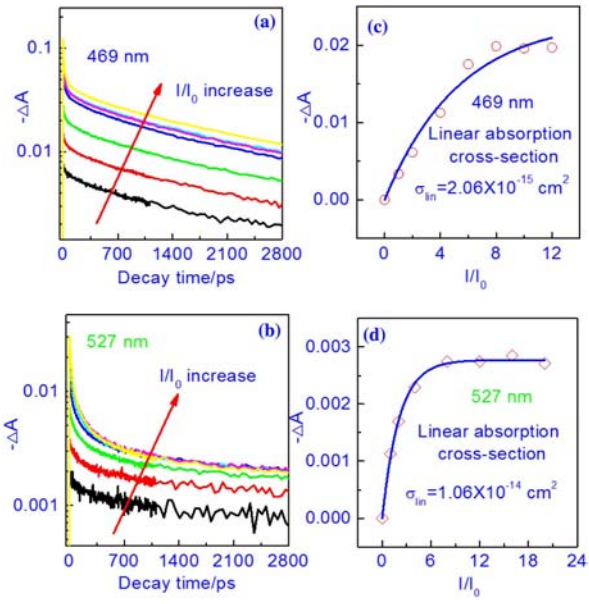

Fig. 3. Excitation intensity-dependent decay traces of the (a) 469 nm and (b) 527 nm 2D NPs. GSB signal amplitude at the time delay of 1 ns, as a function of the excitation intensity of the (c) 469 nm and (d) 527 nm 2D NPs. The curves are the best fits based on Eq. (1).

light intensity used [19]. The GSB signal amplitudes of the 469 nm and 527 nm 2D NPs, for different excitation light intensities, were collected for the decay time of 1 ns, and the results are shown in Figs. 3(c) and 3(d). According to Eq. (1), the σ_{lin} values for the 469 nm and 527 nm 2D NPs were 2.06×10^{-15} cm^2 and 1.06×10^{-14} cm^2, respectively, at 350 nm. The much larger linear absorption cross-section of the 527 nm 2D NPs appears because their volumes (1252 nm^3) are much larger than those of the 469 nm 2D NPs (359 nm^3).

The UV-Vis linear absorption spectra of these 2D NPs indicate that they are likely to absorb multiple photons with their conduction bands filled under the femtosecond-pulse excitation in the 720–2400 nm wavelength range. The incident power-dependent PL spectra of the 469 nm and 527 nm 2D NPs were measured under the excitations at 800 nm, 1300 nm, 1800 nm, and 2200 nm [Fig. 4(a)]. It was found that the multiphoton-excited PL of the 469 nm and 527 nm 2D NPs exhibited a 7-nm-wavelength redshift with respect to their one-photon counterparts, which is likely owing to the reabsorption effect and size inhomogeneity [7]. Furthermore, the slopes indicating the order of the absorption process can be deduced from the relationship between the excitation intensity and multiphoton-excited PL intensity across different excitation wavelengths, as shown in Fig. 4(b). In the short-wavelength range, from 720 nm to 880 nm, the PL slopes for the 2D NPs were ~2, clearly indicating 2PA. As the excitation wavelength was varied from 1200 nm to 1500 nm, the slopes increased to ~3, indicating the dominance of the 3PA process in this wavelength range. The slopes were ~4 for the excitation wavelength in the 1600–1800 nm range, stressing the action of the 4PA mechanism. Finally, the 5PA mechanism was confirmed for the excitation wavelength in the 2200–2400 nm range, and the slopes were ~5. The 2D NPs can produce bright PL emission under the excitation wavelength in the 720–2400 nm range [insets in Fig. 4(b)], indicating they should have large MPA. Therefore, as shown in Fig. 5, the 2PA to 5PA spectra of the 469 nm and 527 nm 2D NPs were determined using the nonlinear transmittance method [20]. Within the region of the 2PA process, the measured 2PA cross-section (σ_2) values were in the range of 0.3–3 × 10^5 GM for the 469 nm 2D NPs and 0.4–4.1 × 10^6 GM for the 527 nm 2D NPs. The maximal σ_2 values were on the upper end of the cross-sections recorded using other semiconductor NCs [4,21]. In the wavelength range of the dominant 3PA process (1200–1500 nm), the maximal 3PA cross-section (σ_3) values of the 469 nm and 527 nm 2D NPs reached ~2.0×10^{-75} cm^6 s^2 photon^{-2} and ~2.3×10^{-74} cm^6 s^2 photon^{-2}, respectively. These values were much larger than those of most PL materials, including CdSe/CdS dot-in-rod heterostructures [22]. For the 4PA process, the maximal 4PA cross-section (σ_4) values obtained were 0.13×10^{-104} cm^8 s^3 photon^{-3} for the 469 nm 2D NPs and 2.06×10^{-104} cm^8 s^3 photon^{-3} at 1600 nm. For the higher-order 5PA cross-section (σ_5) values, the maximal values were determined 0.12×10^{-136} cm^{10} s^4 photon^{-4} for the 469 nm 2D NPs and 1.50×10^{-136} cm^{10} s^4 photon^{-4} at 2200 nm. For all the 2PA to 5PA processes, the 527 nm 2D NPs exhibited significantly larger MPA cross-sections than the 469 nm NPs. This was likely owing to their significantly larger volumes, which enhance both linear absorption and MPA.

Because only a few studies addressed the 4PA and 5PA processes in nonlinear optical materials, direct comparisons of the 4PA and 5PA cross-sections across perovskite 2D NPs and conventional organic dyes and inorganic semiconductor NCs were not convenient. However, based on the existing literature, it is remarkable that the maximal σ_4 and σ_5 values of the 527 nm 2D NPs were 3–8 orders higher than those of specially designed organic molecules, including p-Terphenyl (σ_4:7.6×10^{-112} cm^8 s^3 photon^{-3} at 1300 nm, σ_5:3.8×10^{-144} cm^{10} s^4 photon^{-4} at 1500 nm, pulse width: 140 fs) [20], (E)-3-(4-(2-(1-hexyl-4-methyl-1H-imidazol-5-yl) vinyl) pyridinium -1-yl)propyl sulphate (σ_5:1.9×10^{-143} cm^{10} s^4 photon^{-4} at 2100 nm, pulse width: <140 fs) [23], Poly(2-methoxy-5-(2′-ethylhexyloxy)-1,4-phenylene vinylene) (σ_4:7×10^{-109} cm^8 s^3 photon^{-3} at 1800 nm, pulse width: 120 fs) [24], metal–organic frameworks (σ_4:4.5×10^{-109} cm^8 s^3 photon^{-3} at 1450 nm, pulse width: <150 fs) [25], dendrimer (σ_4:2.1×10^{-107} cm^8 s^3 photon^{-3} at 1600 nm, pulse width: 130 fs) [26], and "star" complexes (σ_4:1.8×10^{-108} cm^8 s^3 photon^{-3} at 1750 nm, pulse width: 130 fs) [27]. In addition, it was found that the maximal 4PA and 5PA cross-sections of the 527 nm

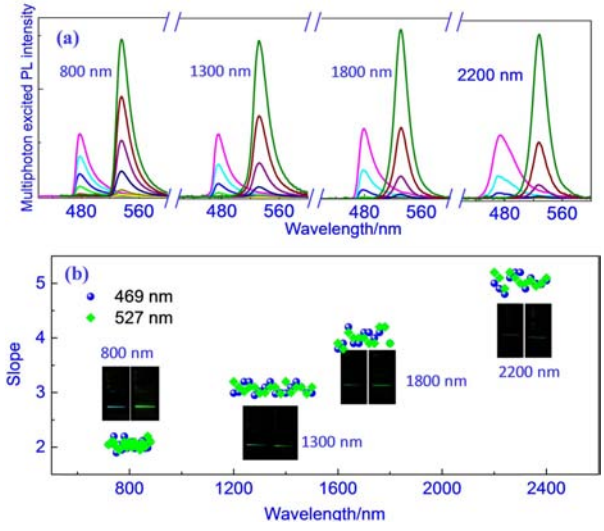

Fig. 4. (a) Incident power-dependent PL spectra of the 469 nm and 527 nm 2D NPs, excited using 800, 1300, 1800, and 2200 nm fs pulses. (b) Wavelength-dependent slope (n) that is defined by the PL intensity that is proportional to the excitation intensity to the power of *n*. Insets: fluorescence photographs of the 2D NPs, taken under multiphoton excitations.

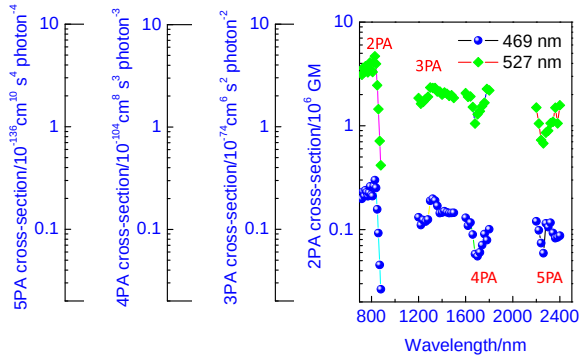

Fig. 5. 2PA to 5PA spectra of the 2D NPs, for the excitation by 100 fs pulses.

2D NPs were 1 order of magnitude smaller compared to those of three-dimensional methylammonium lead bromide/two-dimensional octylammonium lead bromide (σ_4:26.1×10^{-104} cm^8 s^3 $photon^{-3}$ at 1550 nm, σ_5:21.7 × 10^{-136} cm^{10} s^4 $photon^{-4}$ at 2050 nm, pulse width: 50 fs) and $CsPbBr_3$ cubic NCs (σ_4:12.7 × 10^{-104} cm^8 s^3 $photon^{-3}$ at 1550 nm, σ_5:11.8 × 10^{-136} cm^{10} s^4 $photon^{-4}$ at 2050 nm), but comparable to those of $CH_3NH_3PbBr_3$ (σ_4:3.6 × 10^{-104} cm^8 s^3 $photon^{-3}$ at 1550 nm, σ_5:2.9 × 10^{-136} cm^{10} s^4 $photon^{-4}$ at 2050 nm) in Ref. [4]. However, it should be noted that, as we mentioned earlier, owing to probably different methods that were used for determining relevant molar concentrations, strictly identical experimental methods (including the excitation wavelength, pulse width, and molar concentration calculation) must be used when comparing the MPA cross-sections of semiconductor NCs across different published studies.

In conclusion, we report the carrier cooling and MPA properties of $CsPbBr_{2.7}I_{0.3}$ 2D NPs. The 2D NPs exhibited 2D confinement effect-induced giant 2PA and 5PA, which can expand the range of potential applications for all-inorganic perovskite 2D NPs, including nonlinear optoelectronics.

Funding. Shenzhen Science and Technology Innovation Commission (JCYJ20170302142433007, JCYJ20180305180553701, KQJSCX20170726145748); Natural Science Foundation of Guangdong Province (2018A030310637).

REFERENCES

1. G. He, L. Tan, Q. Zheng, and P. Prasad, Chem. Rev. **108**, 1245 (2008).
2. A. Mandal, S. Sreejith, T. He, S. Maji, X. Wang, S. Ong, J. Joseph, H. Sun, and Y. Zhao, ACS Nano **9**, 4796 (2015).
3. Y. Wang, X. Li, X. Zhao, L. Xiao, H. Zeng, and H. Sun, Nano Lett. **16**, 448 (2015).
4. W. Chen, S. Bhaumik, S. A. Veldhuis, G. Xing, Q. Xu, M. Grätzel, S. Mhaisalkar, N. Mathews, and T. Sum, Nat. Commun. **8**, 15198 (2017).
5. Y. Xu, Q. Chen, C. Zhang, R. Wang, H. Wu, X. Zhang, G. Xing, W. W. Yu, X. Wang, Y. Zhang, and M. Xiao, J. Am. Chem. Soc. **138**, 3761 (2016).
6. G. Nagamine, J. O. Rocha, L. G. Bonato, A. F. Nogueira, Z. Zaharieva, A. A. R. Watt, C. H. de Brito Cruz, and L. A. Padilha, J. Phys. Chem. Lett. **9**, 3478 (2018).
7. J. Chen, P. Chábera, T. Pascher, M. E. Messing, R. Schaller, S. Canton, K. Zheng, and T. Pullerits, J. Phys. Chem. Lett. **8**, 5119 (2017).
8. T. He, J. Li, X. Qiu, S. Xiao, C. Yin, and X. Lin, Adv. Opt. Mater. **6**, 1800843 (2018).
9. S. Chen and G. Shi, Adv. Mater. **29**, 1605448 (2017).
10. T. Zhang, M. Dar, G. Li, F. Xu, N. Guo, M. Grätzel, and Y. Zhao, Sci. Adv. **3**, e1700841 (2017).
11. Q. Akkerman, S. Motti, K. Srimath, K. E. Mosconi, V. D'Innocenzo, G. Bertoni, S. Marras, B. Kamino, L. Miranda, F. De Angelis, A. Petrozza, M. Prato, and L. Manna, J. Am. Chem. Soc. **138**, 1010 (2016).
12. B. J. Bohn, Y. Tong, M. Gramlich, M. L. Lai, M. Döblinger, K. Wang, R. L. Z. Hoye, P. Müller-Buschbaum, S. D. Stranks, A. S. Urban, L. Polavarapu, and J. Feldmann, Nano Lett. **18**, 5231 (2018).
13. M. Price, J. Butkus, T. Jellicoe, A. Sadhanala, A. Briane, J. Halpert, K. Broch, J. Hodgkiss, R. Friend, and F. Deschler, Nat. Commun. **6**, 8420 (2015).
14. J. Butkus, P. Vashishtha, K. Chen, J. Gallaher, K. S. Prasad, D. Metin, G. Laufersky, N. Gaston, J. Halpert, and J. Hodgkiss, Chem. Mater. **29**, 3644 (2017).
15. J. Yang, X. Wen, H. Xia, R. Sheng, Q. Ma, J. Kim, P. Tapping, T. Harada, T. W. Kee, and F. Huang, Nat. Commun. **8**, 14120 (2017).
16. M. Li, J. Fu, Q. Xu, and T. Sum, Adv. Mater. 1802486 (2019).
17. M. J. Li, S. Bhaumik, T. W. Goh, M. S. Kumar, N. Yantara, M. Grätzel, S. Mhaisalkar, N. Mathews, and T. C. Sum, Nat. Commun. **8**, 14350 (2017).
18. V. Klimov, P. H. Bolivar, and H. Kurz, Phys. Rev. B **52**, 4728 (1995).
19. J. Chen, K. Zidek, P. Chabera, D. Liu, P. Cheng, L. Nuuttila, J. Al-Marri, H. Lehtivuori, H. Messing, K. Han, K. Zheng, and T. Pullerits, J. Phys. Chem. Lett. **8**, 2316 (2017).
20. T. Yatsuhashi, S. Ichikawa, Y. Shigematsu, and N. Nakashima, J. Am. Chem. Soc. **130**, 15264 (2008).
21. R. Gui, H. Jin, Z. Wang, and L. Tan, Coord. Chem. Rev. **338**, 141 (2017).
22. G. Xing, S. Chakrabortty, S. W. Ngiam, Y. Chan, and T. C. Sum, J. Phys. Chem. C **115**, 17711 (2011).
23. Q. Zheng, H. Zhu, S. Chen, C. Tang, E. Ma, and X. Chen, Nat. Photonics **7**, 234 (2013).
24. B. D. S. Corrêa, L. D. Boni, D. T. Balogh, and C. R. Mendonça, Adv. Mater. **19**, 2653 (2007).
25. H. Quah, W. Chen, M. K. Schreyer, H. Yang, M. Wong, W. Ji, and J. J. Vittal, Nat. Commun. **6**, 7954 (2015).
26. P. V. Simpson, L. A. Watson, A. Barlow, G. Wang, M. P. Cifuentes, and M. G. Humphrey, Angew. Chem. (Int. Ed.) **128**, 2433 (2016).
27. T. Schwich, A. Barlow, M. P. Cifuentes, J. Szeremeta, M. Samoc, and M. G. Humphrey, Chem. Eur. J. **23**, 8395 (2017).